Biosynthesis of Zinc Oxide Nanoparticles Using Averrhoa Bilimbi Fruit Extract: Deagglomeration and Antibiofilm Activity Measurements

Tjokorde Walmiki Samadhi (twsamadhi@cheitb.id)
Bandung Institute of Technology
Vita Wonoputri
Bandung Institute of Technology
Shafira Khairunnisa
Bandung Institute of Technology
Eka Rahayu
Bandung Institute of Technology

Research Article

Keywords: biosynthesis, nanoparticle, ZnO, antibacterial, antibiofilm, plant extract

Posted Date: December 6th, 2023

DOI: https://doi.org/10.21203/rs.3.rs-3658518/v1

Additional Declarations: No competing interests reported.

Abstract

Zinc oxide nanoparticle was biosynthesized using *Averrhoa bilimbi* fruit extract as reducing and capping agent, with a focus on the impact of in-situ deagglomeration method on physical properties and pathogenic inhibition activity against *Escherichia coli* biofilm. Biosynthesis variables included deagglomeration method (ultrasonication vs. PVA as deagglomerant), temperature (30, 60 °C), and zinc precursor/plant extract volumetric ratio (1:2, 2:1). Upon calcination at 375 °C, crystalline ZnO nanoparticles with high phase purity were obtained. The final product formed soft agglomerates, as indicated by hydrodynamic mean particle diameters of 1.0-3.5 mm compared against mean individual particle diameter of 22 nm. Chemical deagglomeration and lower precursor/extract ratio promoted smaller agglomerates. Interaction between deagglomeration method and biosynthesis temperature implied that physical deagglomeration was more effective at higher temperature while the opposite applied for chemical deagglomeration. Antibiofilm activity of the nanoparticles was indicated by an average *E. coli* population reduction of 61% at 50 ppm ZnO dose, which increased to 78% at 200 ppm dose. Lower biosynthesis temperature and precursor/extract ratio increased antibiofilm activity, likely due to higher availability of residual plant extract biomolecules in the final ZnO nanoparticle product. Deagglomeration method did not directly impact the activity. However, the combination of chemical deagglomeration and higher ZnO dose produced a synergistic effect in inhibiting the *E. coli* biofilm growth. Overall, ZnO nanoparticle synthesized using *Averrhoa bilimbi* fruit extract exhibited promising antimicrobial activity against *E. coli*.

1. Introduction

Nanoparticles exhibit physico-chemical properties that are distinct and unique compared to their respective microparticles. This uniqueness stems from their particle size range, within which thermal, optical, mechanical, magnetic, and catalytic properties vary substantially with their size. By modifying particle size distribution and morphology on the nanoscale, materials with customized properties may be engineered to fit specific requirements [1,2]. Zinc oxide has been widely studied as nanoparticles since it is safe, inexpensive, non-toxic, and relatively easy to produce. In the nanoparticle form, ZnO exhibits optical, catalytic, and UV radiation resistance that are generally superior compared to many other oxide nanoparticles [3]. As a semiconductor material, ZnO nanoparticles can be modified for applications as sensors for pollutants and pathogens [4]. Due to the classification of ZnO as GRAS (generally regarded as safe) by the US Food and Drug Administration (21CFR182.8991), a major current direction in ZnO nanoparticle research has been in medicine, namely as antimicrobial agent, drug delivery systems, and bioimaging probe [5].

In general, microbial inactivation by nanoparticle as described by Herman and Herman [6] includes the following steps:

1. Disintegration of cell membrane, which increases the membrane permeability.
2. Disruption of bacterial cell walls or membranes

3. Release of ions from nanoparticles that interact with intracellular and extracellular components
4. Photocatalytic production of reactive oxygen species (ROS) that may disrupt cellular components
5. Inhibition of enzymatic ativities and DNA synthesis
6. Disruption of energy transduction process

For ZnO in particular, the predominant antimicrobial mechanism is the production of ROS that induces oxidative stress against the microbial cells. In addition to increasing ROS production, metallic cations slowly released by oxide nanoparticles can be captured by microbial cells. Suspended ZnO nanoparticles release Zn^{2+} cations in acidic or basic media. These cations form bonds with proteins, carbohydrates, and other critical biocomponents originating from bacteria [7]. Metallic cations that diffuse into the intracellular space may interact with functional groups in proteins and nucleic acids such as amino (-NH), mercapto (-SH) and carboxyl (-COOH) groups. These interactions may result in the damage of enzymatic activity, altering the cellular structure, disrupting physiological processes of the microbe [8]. The positively charged zinc cations may neutralize the electrostatic charge of the lipopolysaccharides within the microbial cell membrane, disrupting the structure of the membrane and inhibiting the growth of bacteria. Moreover, the abrasive nature of the metal cation may cause mechanical damage to the bacterial cell membrane surface such, subsequently causing cell lysis [9].

Analogous to other metal oxides, ZnO nanoparticles may be produced through physical, chemical, and biological routes. The latter, often referred to as biosynthesis, offers several distinct advantages. It is relatively easy to implement with simple equipment and procedures and does not use potentially harmful substances. Biosynthesis by precipitation method usually involves the precipitation of metal ions by biomolecules that are present in a variety of biological agents, which also stabilize the formed nanoparticles [10,11,12].

Numerous biological agents, such as bacteria, fungi, yeast, and viruses can be used in the biological synthesis of nanoparticles. However, these agents require intensive cell maintenance measures which prolong their incubation time. In this regard, biosynthesis using plant extracts as reducing and capping agents is more advantageous. Phytochemicals commonly present in plants can reduce metal ions more rapidly than microbes. Moreover, plants tend to be non-pathogenic and contain more biomolecules [13,14]. A previous work has identified the feasibility of using fruit pulp extract of *Averrhoa bilimbi* for the biosynthesis of zinc nanoparticles [15]. This tree species is widespread in Indonesia, where its fruits are commonly cooked in various dishes. It has been identified to have rich antioxidants that are useful in nanoparticles synthesis, such as alkaloid, phenols, flavonoids, saponins, and tannin [16]. While the work by Rahayu [15] has confirmed the antimicrobial activity of the biosynthesized nanoparticles, it has also identified agglomeration as a major concern.

The strong tendency of zinc nanoparticles synthesized using *Averrhoa bilimbi* extract to agglomerate has been hypothesized to be the cause of antimicrobial activity decrease at higher nanoparticle dose, in which agglomeration reduces the effective surface area of the nanoparticles [15]. A similar decrease of activity at higher nanoparticle dose was also reported by Rokbani et al. [17]. Agglomeration inhibits

contact and penetration of nanoparticles into the bacterial cells, so that the amount of Zn^{2+} cations released into the cells is not sufficient to impart toxic effects on the bacteria. If the agglomerates become overly dense and heavy, nanoparticle sedimentation may occur which reduces the effective concentration of nanoparticles in the suspended state below its total dose [18].

In general, agglomeration of nanoparticles may be caused by high particle reactivity, resulting in large interactions between particles such as Van der Waals force to form solidified particle clusters. Nanoparticle agglomeration may occur during the synthesis process or when the nanoparticle powder is dispersed in a solvent [19]. In biosynthesis, biomolecules perform as capping agents that envelop nanoparticles and increase electrostatic repulsion between particles, thus reducing nanoparticle agglomeration [20]. However, nanoparticles that have been covered by biomolecules may agglomerate due to the high active surface area of the particles [21,22]. Khairunnisa et al. [22] noted that literature on the relationship between agglomeration and biosynthesis process variables is still somewhat scarce. Moulton et al. [23] argued that system temperature and period of nanoparticle aging in dispersion system affect the degree of agglomeration. Mohammadi and Ghasemi [24] argued that improper setting of biosynthesis process variables, namely pH, temperature, and plant extract concentration, may produce larger ZnO nanoparticle agglomerates. Manipulating these variables is then likely to impact agglomeration behavior of biosynthesized ZnO nanoparticles.

Published research works on nanoparticle biosynthesis tend to focus on the ability of various biological agents in reducing metal cations to produce nanoparticles. On the other hand, research specifically addressing the agglomeration issue in biosynthesis is still scarce. A more broadly studied approach in agglomeration control involves the implementation of deagglomeration measures as the biosynthesis proceeds to break down formed agglomerates. In general, these deagglomeration methods can be categorized into physical and chemical methods. Physical deagglomeration may be undertaken by high intensity agitation, vortex mixing, or ultrasonication. Of these methods, ultrasonication has been recognized as the most effective [25]. In this method, mechanical vibration imparted on the suspension media induces intensive interparticle collisions which break apart agglomerates [26]. On the other hand, chemical deagglomeration relies on adding dispersants that increase interparticle repulsion and/or steric hindrance which increases the stability of the nanoparticle suspension. Ideally, for antimicrobial or medicinal applications these dispersants should be non-toxic and do not compromise the performance of the oxide nanoparticles [25]. Polymeric materials such as polyvinyl alcohol (PVA) can be applied to nanoparticles to increase repulsion and steric hindrance. A study stated that PVA could maintain an adequate stability of metal nanoparticle solutions for up to 3 months at room temperature storage [27]. PVA has also been examined on the biosynthesis of numerous metal nanoparticles and has been proven to reduce the level of nanoparticles agglomeration [28,29].

The greater the intensity of deagglomeration method applied, the greater the deagglomeration effect that occurs. However, a study discovered deagglomeration measures beyond a particular level of intensity do not provide further stability improvement or even increase the occurrence of re-agglomeration [30]. Intensity of deagglomeration treatment should be determined carefully to prevent re-agglomeration with

efficient use of raw materials and energy during the synthesis process. This current study attempted to compare the effectiveness of physical and chemical deagglomeration, along with the modification of synthesis conditions aimed at improving the stability of biosynthesized ZnO nanoparticles using *Averrhoa bilimbi* fruit extract. The effect of deagglomeration on the reactivity of ZnO nanoparticles was evaluated by measuring their antimicrobial activities.

2. Materials and Methods

2.1. Biosynthesis of ZnO Nanoparticles

Fresh *Averrhoa bilimbi* fruits were obtained from a traditional market in the city of Bandung. These were washed by demineralized water and manually ground into a pulp using mortar and pestle. The pulp was then mixed with demineralized water and fed to a three-neck glass flask at a pulp to water ratio of 1:10 (w/v). Extraction was undertaken by reflux method at 70 °C for 90 minutes. The reflux product was left to cool down to ambient temperature and clarified using a filter paper. The extract stock was stored in a refrigerator at 4 °C prior to use.

The biosynthesis experiment incorporating deagglomeration was conducted using a full factorial design with three factors, each varied at two levels (2^3 full factorial design). The factor levels of this experiment are described in Table 1. This experiment therefore combined one categorical factor (deagglomeration method, X_1) and two quantitative factors (synthesis temperature, X_2 and precursor/extract volumetric ratio, X_3). Zinc nitrate precursor solution concentration was kept at 0.05 M. Polyvinyl alcohol (PVA) solution was selected as the chemical deagglomerant, which was prepared by dissolving in demineralized water at 1% (wt) concentration, followed by heating under constant agitation at 90 °C for 1 hour. Each run combination was conducted in three replicates.

Table 1 Factor Levels of Deagglomeration Experiment

Experimental factors	Notation	Values of levels	
		(-1) or low	(+1) or high
Deagglomeration method	X_1	Chemical	Physical
Synthesis temperature (°C)	X_2	30	60
Precursor/extract volumetric ratio	X_3	1:2	2:1

Synthesis involving physical deagglomeration was conducted within an ultrasonicator bath. A glass beaker containing the zinc precursor solution was immersed in the ultrasonicator and heated to the prescribed temperature. The fruit extract was then added dropwise to the precursor solution to obtain the prescribed precursor to extract volume ratios. The sonication was maintained throughout the reaction duration. On the other hand, synthesis involving chemical deagglomeration was conducted by placing the reactor on a heating plate. The precursor solution was heated to the prescribed temperatures. The fruit

extract was then added dropwise under constant agitation at 500 rpm. Dropwise addition of 1% PVA solution was initiated 5 minutes after the fruit extract addition was completed, at a PVA solution to zinc nitrate precursor solution volume ratio of 1:10.

Reaction suspension mixtures obtained after the biosynthesis via the two routes described previously were aged for 18 hours at ambient temperature to increase the amount of nanoparticles precipitate. The aged suspension was then centrifuged at 10,000 rpm and 15 minutes, washed with demineralized water and re-centrifuged. The final precipitates were then dried at 80 °C and calcined for 1 hour at 450 °C. This calcination temperature was determined by analyzing a specimen obtained in a preliminary experiment using a simultaneous TGA-DSC unit (Linseis STA PT1600, Analytical Instrumentation Laboratory, Chemical Engineering Department at Institut Teknologi Bandung). The calcined products were then manually ground using mortar and pestle and stored in airtight containers prior to characterization.

2.2. Physical Characterization

Identification of crystalline phases and degree of crystallinity were determined by X-ray diffraction (XRD) with Cu-Ka radiation source set at 2q diffraction angle range of 10-80 degrees (Bruker D8, Analytical Instrumentation Laboratory, Department of Chemical Engineering in Institut Teknologi Bandung). One specimen was used for this phase characterization, namely the ZnO nanoparticle produced at zinc nitrate precursor to fruit extract volumetric ratio of 1:2, synthesis temperature of 60 °C without deagglomeration treatment. The diffraction pattern of the specimen was compared against the standard pattern JCPDS No. 00-036-1451 [31].

Nanoparticle size distribution was measured by laser dynamic laser scattering (DLS), which relies on the correlation between intensity of scattered laser beam and size of particles under Brownian motion (Horiba SZ-100, Nanoparticle and Nanotechnology Research Center at Institut Teknologi Bandung). Sample preparation involved the suspension of 0.001 g nanoparticle specimen in 10 mL of demineralized water, followed by sonication for 15 minutes. The homogenized suspension was then injected into a cuvette and analyzed at laser wavelength of 633 nm and detector angle of 173 degree.

Nanoparticle morphology was characterized using a TEM unit (Hitachi HT-7700, Nanoparticle and Nanotechnology Research Center at Institut Teknologi Bandung). In the TEM characterization, nanoparticle specimens were suspended in analytical grade ethanol, dripped on a copper specimen grid holder. The specimen drop was left in a protected environment to evaporate the ethanol. Micrographs from several select specimens were also analyzed using ImageJ freeware to determine their particle size distribution, for comparison with DLS results.

2.3. Antimicrobial Activity Measurement

Antimicrobial activity of ZnO nanoparticles produced by the main experiment in Table 1 was measured against *Escherichia coli* ATCC 25922 as a biofilm culture. In this form, bacterial colonies are grown on

solid surface and are encased in extracellular polymeric substance (EPS). Thus, the the antimicrobial activity measured in this mode is commonly referred to as antibiofilm activity.

The inoculum was prepared from a single colony of *E.coli* grown on Nutrient Agar (NA), which was then added into 5 mL of Luria Bertani (LB; 10 g/L tryptone, 5 g/L yeast extract, and 10 g/L NaCl) medium and incubated overnight at 30 °C, 150 rpm. For the antibiofilm assay, 1 ml of the overnight inoculum was added into 50 mL of M9 minimal salt growth medium (48 mM Na_2HPO_4, 22 mM KH_2PO_4, 9 mM NaCl, 19 mM NH_4Cl, 2 mM $MgSO_4.7H_2O$, 100 mM $CaCl_2$ and 20 mM glucose) to trigger the formation of biofilm.

Similarly, each well in the 24-well plate was filled with 0.9 mL bacterial aliquots and 0.1 mL of ZnO suspension at a specific concentration. The well plate was then incubated at 37 °C, 180 rpm for 4.5 hours. The supernatant was then carefully removed, and the biofilm was then washed with 1.75 mL phosphate buffered saline (PBS) solution. Quantification of the biofilm was performed by staining using 1 mL of 0.1% crystal violet solution followed by incubation for 15 minutes. The excess crystal violet solution was washed off, and the remaining stain was re-dissolved in 1.75 mL analytical grade ethanol. Absorbances of resulting solutions were analyzed measured at 570 nm (OD570). Measured values obtained from wells with ZnO addition were normalized against OD570 of the positive control and denoted as the residual *E. coli* population in the biofilm.

Two levels of ZnO nanoparticle dose (50 and 200 ppm with respect to the total suspension volume in each well) were studied, along with the three experimental factors outlined in Table 1. This addition effectively expanded the experiment into a full factorial 2^4 design. Factor levels of the antibiofilm activity experiment are summarized in Table 2.

Table 2 Factor Levels of Antibiofilm Activity Experiment

Experimental factors	Notation	Values of levels	
		(-1) or low	(+1) or high
Deagglomeration method	X_1	Chemical	Physical
Synthesis temperature (°C)	X_2	30	60
Precursor/extract volumetric ratio	X_3	1:2	2:1
ZnO nanoparticle dose (ppm)	X_4	50	200

3. Results and Discussion

3.1. Biosynthesis and Characterization of ZnO Nanoparticles

A specimen from a preliminary experiment (precursor/extract volume ratio 1:2, synthesis temperature 60 °C for 3 hours, followed by oven drying at 80 °C) was subjected to simultaneous TGA/DSC analysis to determine the appropriate calcination temperature of the as-dried nanoparticles for the entire main experiment. The thermal analysis employed heating from 50 to 600 °C at 10 °C/min heating rate. Figure 1 presents the thermogram of this specimen. Mass loss due to evaporation of moisture occurred in the 100–160 °C range, resulting in an approximately 20% mass loss. A rapid and large mass loss accompanied by a sharp endothermic peak occurred in the 370–405 °C range, producing a mass loss of roughly 50%. This thermal event is associated with the conversion of zinc hydroxide and/or zinc hydroxynitrate into ZnO, and the burn-off of organic matter in the residual fruit extract [32, 33, 34]. Thus, a calcination temperature of 375 °C was selected for all runs in the main experiment.

Figure 2 presents the X-ray diffractogram of a nanoparticle specimen produced in the preliminary experiment at precursor/extract volumetric ratio of 1:2, synthesis temperature of 60 °C without deagglomeration treatment. Comparison with reference diffraction pattern indicated that the formation of ZnO is complete after calcination at 375 °C for 1 hour. Phase purity of the specimen is very good, with negligible presence of crystalline impurities.

The 2^3 full factorial design matrix of the main experiment is summarized in Table 3 based on factor level settings in Table 1. Two key particle size distribution parameters measured by the DLS method are included in the table, namely particle mean hydrodynamic diameter and polydispersity index (PDI). Each run was replicated three times; particle diameter and PDI values in the table are averages of these three replicates. The mean diameter was measured in the 1.0-3.5 μm range, indicating that despite the deagglomeration measures implemented, agglomeration of ZnO nanoparticles still occur. PDI values averaged over the replicates were in the 0.9–3.9 range. The measured values in Table 3 therefore also suggest that agglomeration persisted, although subsequent morphological characterization by TEM suggested that the ZnO nanoparticle specimens formed soft agglomerates.

Table 3
Particle measurement results by DLS method of the main biosynthesis main experiment

Run No.	Deagglomeration method (X_1)	Synthesis T, °C (X_2)	Precursor/extract volume ratio (X_3)	Hydrodynamic mean diameter (nm)	PDI
1	Chemical	30	0.5	1169	2.96
2	Physical	30	0.5	3337	1.79
3	Chemical	60	0.5	2987	1.10
4	Physical	60	0.5	1494	1.73
5	Chemical	30	2.0	3093	1.01
6	Physical	30	2.0	3534	1.12
7	Chemical	60	2.0	3164	1.00
8	Physical	60	2.0	3151	0.88

Results of ANOVA treatment using all possible main and interaction effects for the particle size measurement data in Table 3 are summarized in Table 4. Hydrodynamic mean diameter, averaged over the three replicates, was measured in the 1.2–3.5 μm range. This particle size range suggests that agglomeration was still present. Varibles significantly influencing this quantity include deagglomeration method and precursor / extract ratio. Regression coefficients for mean particle diameter data suggest that smaller particles may be achieved by using chemical deagglomeration and lower precursor / extract volume ratio. Synthesis temperature also influences particle mean diameter through antagonistic binary interactions with deagglomeration method (X_1X_2). The negative coefficient of this interaction implies that smaller particles may be produced by combining chemical deagglomeration (low level of X_1) and lower synthesis temperature (low level of X_2). The three-way interaction is statistically highly significant with P-value less than 0.01. This implies that all lower-order effects cannot be eliminated from the ANOVA regression according to the hiearchy principle, including those with P-value higher than the prescribed significance level.

The smaller particle obtained at lower precursor / extract ratio was also observed by Skandalis et al. [35]. These authors reported that a twofold increase of extract volume reduces nanoparticle diameter from 50–60 nm to 40 nm. At lower extract volume, these authors argued that Zn cation reduction proceeds slower due to reduced availability of biomolecules responsible for the reduction and capping of nanoparticles. The slow formation of nanoparticle nuclei allows more time for agglomerates to form.

ANOVA results in Table 4 indicates a significant interaction between deagglomeration method and synthesis temperature, such that the effectiveness of physical deagglomeration occurs at higher (60 °C) temperature. Similar result was reported by Kandjani et al. [36]. ZnO synthesis using sonication at 50 °C produced agglomerates with hydrodynamic diameters in the 2.5–4.5 μm range, while the same procedure held at 70 °C synthesis temperature reduced the agglomerate diameters to 1.5-3.0 μm. Higher

temperature increases solubility of nanoparticle precursors, thereby shifting the reacting system away from supersaturation of the precursors and delaying the formation of agglomerates. Tran et al. [37] reported that in biosynthesis using the ultrasonication method, concentration of precursor affects the diameter of the nanoparticles. Synthesis at Zn^{2+} concentration of 0.001 M produced ZnO nanoparticle hydrodynamic diameter of 112.9 nm and PDI of 0.330. Increasing the Zn^{2+} concentration to > 0.01 M increased the ZnO diameter to > 3000 nm and PDI > 1.0.

On the other hand, chemical deagglomeration using PVA was found to be more effective at lower synthesis temperature. PVA contains acetate groups that can be ionized at lower pH. In acidic environment (pH = 3), the negatively charged acetate forms electrostatic bond with metal cations on the nanoparticle surface. When pH increases approaching neutral (pH = 6), the degree of ionization of acetate decreases, thereby decreasing the adsorption of PVA on particle surface [38]. In this current work, an increase in temperature combined with chemical deagglomeration produced larger agglomerates. This is perhaps due to the PZC (pH at point of zero electrostatic charge) of ZnO which is in the pH = 8–9 range, while the pH during biosynthesis was in the vicinity of 2.5. This causes the nanoparticle surface to be dominated by positive charge. Attraction between the positively charged nanoparticle and negatively charged acetate groups causes the PVA macromolecule to curl, effectively reducing the layer of PVA adsorbed on the particle surface. Increase in temperature increases ionization of acetate groups, thereby further reducing the PVA adsorption layer and inducing nanoparticle ionization [39, 40].

The measured PDI values listed in Table 3 – averaged over the three replicates – were in the 0.88–2.96 range. PDI values in the 0.1–0.25 range generally indicate monodispersed or uniformly sized particles, while values larger than 0.7 indicate non-uniformly sized particles [41]. PDI values in Table 3 are consistent with the mean particle diameters in the same table, which suggests that substantial agglomeration of the ZnO nanoparticles still occurred. Significant variables impacting PDI according to Table 4 are synthesis temperature and precursor / extract volume ratio. The negative coefficients of these factors imply that more uniformly sized particles (lower PDI) may be achieved by selecting higher synthesis temperature and higher precursor / extract ratio. Two two-way interactions are significant, namely X_1X_2 and X_2X_3; both are synergistic. Analogous to the mean particle diameter data, the three-way interaction also significantly influences PDI.

Table 4
Full-model ANOVA statistical treatment results of biosynthesized particle size measurement data

Source of variance	Mean hydrodynamic diameter			PDI		
	Coefficient (coded variables)	F_0	P-value	Coefficient (coded variables)	F_0	P-value
X_1 (Deag. Method)	138.0	20.41	< 0.000	-0.071	1.39	0.255
X_2 (Synthesis T)	-42.1	1.90	0.187	-0.272	20.76	< 0.000
X_3 (Precursor/extract)	494.4	262.15	< 0.000	-0.447	56.11	< 0.000
X_1X_2	-514.4	283.80	< 0.000	0.196	10.83	0.005
X_1X_3	-31.0	1.03	0.326	0.067	1.24	0.281
X_2X_3	-35.7	1.37	0.259	0.207	12.00	0.003
$X_1X_2X_3$	401.0	172.43	< 0.000	-0.254	18.13	0.001
Coeff. of correlation						
R^2	97.89%			88.27%		
R^2_{adj}	96.97%			83.14%		

Figures 3 through 6 present TEM images of several specimens of ZnO nanoparticle final products after calcination. These were taken from run numbers 2, 3, 5, and 8 in Table 3. Individual ZnO nanoparticles with sizes in the order of 10–50 nm are clearly identifiable in all images, exhibiting hexagonal geometry of the wurtzite ZnO structure. Cuboidal and spherical shaped individual particles are also observed. Figures 3b, 4b, 5b, and 6b indicate that ZnO particles were clumped together in large, soft agglomerates. This explains the micrometer mean particle size and broad particle size distribution measured by DLS as summarized in Table 3. Agglomeration may be induced during TEM sample preparation by the drop casting method, in which nanoparticle specimens are suspended in ethanol and dropped on a sample grid. The droplet-containing grid is then left standing to allow the solvent to evaporate, during which particles may coalesce and form soft agglomerates due to high particle surface energy [42].

To confirm the approximate dimensions of individual particles, image analysis using the ImageJ freeware was conducted on specimen from Run no. 5. The mean individual particle size was measured at 22.38 nm, with a standard error of 0.99 nm. Figure 7 presents the particle size distribution produced by image analysis of specimen from Run no. 5. The particle size detected by image analysis is much smaller than the DLS results, suggesting that the image analysis indeed measured individual ZnO nanoparticles

instead of agglomerates. This individual ZnO nanoparticle size is comparable to values reported in Rakgotho et al. [43], where ZnO nanoparticle synthesized using sorghum seeds exhibited individual particle diameters in the 20–30 nm range after calcination, as observed by TEM.

3.2. Measurement of Antimicrobial Activity

By adding ZnO nanoparticle dose (50 and 200 ppm) in the antibiofilm activity assay as an experimental factor, the 2^3 experiment in Table 3 was expanded to 2^4 full factorial experiment. Each run in this experiment was replicated three times. Table 5 summarizes the design matrix of this experiment. Response variables in the table are residual *E. coli* biofilm population as inferred from OD600 of bacteria-containing supernatant specimens normalized against OD600 value of the control (no added ZnO nanoparticles) assay. Residual bacterial populations listed in the table are average values taken from three replicates in each run.

Table 5
Design matrix and results of antibiofilm activity measurements of biosynthesized ZnO nanoparticles against *E. coli*

Run No.	Deagglomeration method (X_1)	Biosynthesis T, °C (X_2)	Precursor/extract (X_3)	ZnO dose, ppm (X_4)	Residual biofilm population, %	Antibiofilm activity, %
1	Chemical	30	0.5	50	14.6	85.4
				200	7.9	92.1
2	Physical	30	0.5	50	20.7	79.3
				200	5.0	95.0
3	Chemical	60	0.5	50	61.2	38.8
				200	22.2	77.8
4	Physical	60	0.5	50	47.5	52.5
				200	20.2	79.8
5	Chemical	30	2	50	39.8	60.2
				200	13.8	86.2
6	Physical	30	2	50	22.1	77.9
				200	28.8	71.2
7	Chemical	60	2	50	58.0	42.0
				200	34.5	65.5
8	Physical	60	2	50	49.9	50.1
				200	39.8	60.2

Figure 8 describes the residual biofilm population of *E. coli* after incubation for 4.5 hours in M9 minimum salts medium, in the presence of biosynthesized ZnO nanoparticles. Error bars in the figure were calculated as standard errors between replicates within each run combination. Figure 7 clearly indicates the increased antibiofilm activity (100% - residual population) as ZnO dose increased from 50 to 200 ppm. The average antibiofilm activity at 50 ppm ZnO was 61% across all runs, which increased to 78% at 200 ppm ZnO. The highest activity was observed in Run no.2 at 200 ppm ZnO dose, namely 95% reduction (or 5% residual) relative to the control case. Overall, the antibiofilm activities of biosynthesized ZnO nanoparticles were higher than those of the commercial ZnO nanoparticle reported by Rahayu et al. [12], which was 32% at 50 ppm and 40% at 200 ppm doses, respectively. As another comparison, Kang et al. [44] reported that the highest anti-biofilm activity against *Pseudomonas aeuruginosa* was 84.69% at a ZnO nanoparticles dose of 512 ppm.

ANOVA treatment results for antibiofilm activity measurement data using a full model (up to the highest-ordered $X_1X_2X_3X_4$ interaction effect) are summarized in Table 6. Pareto plot of effects in the full-model ANOVA at 95% confidence level is presented in Fig. 9. This plot indicates that high-order (three-way and four-way) interactions did not impact the antibiofilm activity in a statistically significant manner. The plot also indicates that two-way X_2X_4 interaction effect is significant, but the X_1X_4 effect is just slightly below the critical t-value at 95% confidence level. All other two-way interaction effects were not significant.

To improve the significance of the overall regression model, a model refinement was then conducted by eliminating three-way and four-way interactions, and two-way interactions with effects far below the critical t-value in Fig. 8. Since the X_1X_4 two-way interaction effect was only slightly lower than the critical t-value in the full-model ANOVA, the confidence level was reduced to 90% in the model refinement.

Table 6
Full-model ANOVA treatment results of antibiofilm activities of biosynthesized ZnO nanoparticles

Source of variance	Coefficient (coded variables)	F_0	P-value
X_1	-1.12	0.49	0.490
X_2	11.28	49.11	< 0.001
X_3	5.46	11.50	0.002
X_4	-8.84	30.20	< 0.001
X_1X_2	-1.19	0.54	0.467
X_1X_3	0.43	0.07	0.792
X_1X_4	3.05	3.59	0.067
X_2X_3	-1.59	0.97	0.332
X_2X_4	-3.63	5.09	0.031
X_3X_4	2.24	1.93	0.174
$X_1X_2X_3$	1.18	0.54	0.468
$X_1X_2X_4$	0.08	0.00	0.963
$X_1X_3X_4$	2.71	2.84	0.102
$X_2X_3X_4$	1.85	1.31	0.260
$X_1X_2X_3X_4$	-2.50	2.41	0.131
Coeff. of correlation			
R^2	77.56%		
R^2_{adj}	67.04%		

Results of this model refinement are summarized in Table 7. Since the interaction X_1X_4 is significant at 90% confidence level, the main effect of X_1 cannot be eliminated according to the hierarchy principle. The positive coefficient of X_2 implies that higher antibiofilm activity (i.e lower residual population) may be achieved by selecting lower biosynthesis temperature. Apart from X_1 that has to be included according to the hierarchy principle, the refined model comprises only statistically significant effects. The values of R^2 and R^2_{adj} indicated reasonably good fit of the ANOVA model to the measurement data. Therefore, this level of refinement was deemed sufficient.

Increased temperatures may cause the deterioration of biomolecules acting as reducing and capping agents, thereby increasing particle agglomeration [24]. Analogously, the positive coefficient of X_3 implies that higher antibiofilm activity is produced at lower precursor / extract ratio, consistent with smaller agglomerates produced by lower ratio as evident in Table 4. The negative value of X_4 coefficient simply confirmed that increasing ZnO dose from 50 to 200 ppm indeed increased the antibiofilm activity.

Since the coefficient of X_1X_4 interaction is negative, and X_4 should be set at its high level to improve antibiofilm activity, then X_1 (deagglomeration method) should be set at its 'low' level according to the design matrix in Table 5, namely the chemical deagglomeration method. The preference for chemical deagglomeration is consistent with results in Table 4, in which chemical deagglomeration produced smaller agglomerates.

Table 7
ANOVA statistical treatment results of residual biofilm population data using the refined regression model

Source of variance	Coefficient (coded variables)	F_0	P-value
X_1	-1.12	0.47	0.498
X_2	11.28	47.24	< 0.001
X_3	5.46	11.06	0.002
X_4	-8.84	29.05	< 0.001
X_1*X_4	3.05	3.45	0.070
X_2*X_4	-3.63	4.89	0.033
Coeff. of correlation			
R^2	70.11%		
R^2_{adj}	65.74%		

Data from the biosynthesis and antibiofilm activity measurement experiments indicated that chemical deagglomeration using PVA was able to produce smaller agglomerates, which also exhibited better antibiofilm activity. Smaller nanoparticles size translates to larger active surface area involved in binding to the biomolecule moieties, which ultimately provides higher antimicrobial activity [45].

Mechanism of microbial inactivation by metal oxide nanoparticles is related to the production of ROS which causes oxidative stress. ROS are natural bioproducts from cell oxidative metabolism which can disrupt redox homeostasis in cells resulting in oxidative stress, affect membrane lipids, and change the structure of DNA and proteins [46]. ZnO can stimulate the production of ROS which causes damage to

almost all organic biomolecules such as amino acids, carbohydrates, lipids, nucleic acids, and proteins resulting in microbial death [9]. ZnO nanoparticles can also interact with biofilms through electrostatic forces between positive metal ions and negative biofilm matrices. Extracellular polymer matrix (EPM) in biofilms has pores that can be filled with solutions with various ion concentrations. Metal ions and polyphenols from the nanoparticles will be distributed in the biofilm by diffusion through the pores. Furthermore, zinc ions interfere with enzymatic activity during peptidoglycan synthesis so that biofilms are difficult to produce from the initial phase of their formation [47, 48].

4. Conclusions

Biosynthesis of ZnO using *Averrhoa bilimbi* fruit extract incorporating physical or chemical deagglomeration measures have been proved to be able to produce ZnO nanoparticles in the hexagonal wurtzite structure with high phase purity and with average individual particle diameter of 22 nm as determined by TEM image analysis. Despite the implementation of deagglomeration measures, soft agglomerates were still evident. The biosynthesis produced ZnO agglomerates with mean hydrodynamic particle diameter of 1.2–3.5 μm and PDI of 0.88–2.96 as measured by laser scattering. Smaller agglomerates may be obtained by chemical deagglomeration using PVA and lower precursor / extract ratio. A statistically significant interaction exists between deagglomeration method and biosynthesis temperature, such that physical deagglomeration was more effective at higher temperature, while chemical deagglomeration is more effective at lower temperature.

Average activity of biosynthesized ZnO nanoparticles against *E. coli* biofilm was measured as 61% at 50 ppm ZnO dose, increasing to 78% at 200 ppm ZnO. Factors that contribute to smaller agglomerates, namely chemical deagglomeration and higher volumetric proportion of plant extract during biosynthesis also produced higher antibiofilm activity. The effect of chemical deagglomeration method appeared through interaction with ZnO dose, in which increased antibiofilm required a combination between chemical deagglomeration and higher ZnO dose. Lower biosynthesis temperature also increased antibiofilm activity, which was hypothesized to be associated with less degradation of biomolecules during the synthesis.

Declarations

Acknowledgments

This research was funded by Institut Teknologi Bandung through the Research, Community Empowerment, and Innovation Program (PPMI ITB) for the Chemical Engineering Product Design and Development Research Group.

Statement of Conflict of Interest

On behalf of all authors, the Corresponding Author states that there is no conflict of interest.

References

1. Manojkumar K, Sivaramakrishna A, Vijayakrishna K. A short review on stable metal nanoparticles using ionic liquids, supported ionic liquids, and poly(ionic liquids). J Nanopart Res. 2016;18:103–1-103 – 22. https://doi.org/10.1007/s11051-016-3409-y
2. Sirelkhatim A, Mahmud S, Seeni A, Kaus NHM, Ann LC, Bakhori SKM, Hasan H, Mohamad D. Review on zinc oxide nanoparticles: Antibacterial activity and toxicity mechanism. Nano-Micro Lett. 2015;7:219–242. https://doi.org/10.1007/s40820-015-0040-x
3. Kalpana VN, Rajeswari VD. A review on green synthesis, biomedical applications, and toxicity studies of ZnO NPs. Bioinorg Chem Appl. 2018;3569758-1-3569758-12. https://doi.org/10.1155/2018/3569758
4. Ul Haq AN, Nadhman A, Ullah I, Mustafa G, Yasinzai M, Khan I. Synthesis approaches of zinc oxide nanoparticles: The dilemma of ecotoxicity. J Nanomater. 2017;8510342-1-8510342-14. https://doi.org/10.1155/2017/8510342
5. Jayaseelan C, Rahuman AA, Kirthi AV, Marimuthu S, Santhoshkumar T, Bagavan A, Gaurav K, Karthik L, Rao KVB. Novel microbial route to synthesize ZnO nanoparticles using Aeromonas hydrophila and their activity against pathogenic bacteria and fungi. Spectrochim Acta A Mol Biomol Spectrosc. 2012;90:78–84. https://doi.org/10.1016/j.saa.2012.01.006
6. Herman A, Herman AP. Nanoparticles as antimicrobial agents: Their toxicity and mechanisms of action. J Nanosci Nanotechnol. 2014;14:946–957. https://doi.org/10.1166/jnn.2014.9054
7. Siddiqi KS, ur Rahman A, Tajuddin, Husen A. Properties of zinc oxide nanoparticles and their activity against microbes. Nanoscale Res Lett. 2018;13:1–13. https://doi.org/10.1186/s11671-018-2532-3
8. Wang L, Hu C, Shao L. The antimicrobial activity of nanoparticles present situation and prospects for the future. Int J Nanomed. 2017;12:1227–1249. https://doi.org/10.2147/IJN.S121956
9. Raghunath A, Perumal E. Metal oxide nanoparticles as antimicrobial agents: a promise for the future. Int J Antimicrob Agents. 2017;49:137–152. https://doi.org/10.1016/j.ijantimicag.2016.11.011
10. Sajjad S, Leghari SAK, Ryma NA, Farooqi SA. Green synthesis of metal-based nanoparticles and their applications. In: Kanchi S, Ahmed S, editors. Green metal nanoparticles: synthesis, characterization and their applications. Hoboken: Wiley; 2018. pp. 23–54.
11. Kim DW, Kim DS, Kim YG, Kim YC, Oh SG. Preparation of hard agglomerates free and weakly agglomerated antimony doped tin oxide (ATO) nanoparticles by coprecipitation reaction in methanol reaction medium. Mater Chem Phys. 2006;97:452–457. https://doi.org/10.1016/j.matchemphys.2005.08.046
12. Rahayu E, Wonoputri V, Samadhi TW. Plant extract-assisted biosynthesis of zinc oxide nanoparticles and their antibacterial application. IOP Conf Ser Mater Sci Eng. 2020;823:012036-1-012036-11. https://doi.org/10.1088/1757-899X/823/1/012036
13. Kumar I, Mondal M, Sakhtivel N. Green synthesis of phytogenic nanoparticles. In: Shukla AK, Iravani S, editors. Green Syhthesis, Characterization and Application of Nanoparticles. Cambridge: Elsevier;

2019. pp. 37–73.

14. Pal G, Rai P, Pandey A. Green synthesis of nanoparticles: A greener apporach of cleaner future. In: Shukla AK, Iravani S, editors. Green synthesis, characterization and applications of nanoparticles. Cambridge: Elsevier; 2019. pp. 1–26.
15. Rahayu E. Synthesis and characterization of ZnO nanoparticles using *Averrhoa bilimbi* fruit extract as antimicrobial agent. Master Thesis, Institut Teknologi Bandung; 2019.
16. Suluvoy JK, Berlin Grace VM. Phytochemical profile and free radical nitric oxide (NO) scavenging activity of *Averrhoa bilimbi* L. fruit extract. 3 Biotech. 2017;7:85–1-85 – 1. https://doi.org/10.1007/s13205-017-0678-9
17. Rokbani H, Daigle F, Ajji A. Combined effect of ultrasound stimulations and autoclaving on the enhancement of antibacterial activity of ZnO and SiO2/ZnO nanoparticles. Nanomaterials. 2018;8:129–1-129 – 17. https://doi.org/10.3390/nano8030129
18. Pradhan S, Hedberg J, Blomberg E, Wold S, Odnevall WI. Effect of sonication on particle dispersion, administered dose and metal release of non-functionalized, non-inert metal nanoparticles. J Nanopart Res. 2016;18:285–1-285 – 14. https://doi.org/10.1007/s11051-016-3597-5
19. Yokoyama T, Masuda H, Suzuki M, Ehara K, Nogi K, Fuji M, Fukui T, Suzuki H, Tatami J, Hayashi K, Toda K. Basic properties and measuring methods of nanoparticles. In: Hosokawa M, Nogi K, Naito M, Yokoyama T, editors. Nanoparticle Technology Handbook. Amsterdam: Elsevier; 2012. pp. 3–48
20. Gulati S, Sachdeva M, Bhasin KK. Capping agents in nanoparticle synthesis: Surfactant and solvent system. AIP Conf Proc. 2018;1953:030214-1-030214-4. https://doi.org/10.1063/1.5032549
21. Shanavas S, Priyadharsan A, Karthikeyan S, Dharmaboopathi K, Ragavan I, Vidya C. Green synthesis of titanium dioxide nanoparticles using *Phyllanthus niruri* leaf extract and study on its structural, optical, and morphological properties. Mater Today Proc. 2020;26:3531–3534. https://doi.org/10.1016/j.matpr.2019.06.715
22. Khairunnisa S, Wonoputri V, Samadhi TW. Effective deagglomeration in biosynthesized nanoparticles: A mini review. IOP Conf Ser Mater Sci Eng. 2021;1143:012006-1-012006-10. https://doi.org/10.1088/1757-899X/1143/1/012006
23. Moulton M, Yu K, Braydich-Stolle L, Schlager J, Schrand A, Hussain S (2008) Effects of temperature, time, and solution on nanoparticle agglomeration, American Physical Society, 2008 Spring Meeting of the Ohio-Region Section of APS, March 28–29, 2008, Youngstown, retrieved from internet: http://meetings.aps.org/link/BAPS.2008.OSS.C2.2, C2.00002
24. Mohammadi FM, Ghasemi N. Influence of temperature and concentration on biosynthesis and characterization of zinc oxide nanoparticles using cherry extract. J Nanostruct Chem. 2018;8:93–102. https://doi.org/10.1007/s40097-018-0257-6
25. Hartmann NB, Jensen KA, Baun A, Rasmussen K, Rauscher H, Tantra R, Cupi D, Gilliland D, Pianella F, Sintes JMR. Techniques and protocols for dispersing nanoparticle powders in aqueous media — is there a rationale for harmonization? J Toxicol Environ Health. 2015; Part B 00:1–28. https://doi.org/10.1080/10937404.2015.1074969

26. Othman SH, Rashid SA, Ghazi TIM, Abdullah N. Dispersion and stabilization of photocatalytic TiO_2 nanoparticles in aqueous suspension for coatings applications. J Nanomatter. 2012;718214-1-718214-10. https://doi.org/10.1155/2012/718214
27. Chandran S, Ravichandran V, Chandran S, Chemmanda J, Chandarshekar B. Biosynthesis of PVA encapsulated silver nanoparticles. J App Res Technol. 2016;14:319–324. https://doi.org/10.1016/j.jart.2016.07.001
28. Mandal P. Green synthesis and characterization of polyvinyl alcohol embedded silver nanoparticles using simul (*Bombax ceiba*) flower extract. Int J Curr Res Rev. 2017;9:3–6. https://doi.org/10.7324/IJCRR.2017.9142
29. Mandal P, Ghosh S. Green synthesis of poly(vinyl alcohol) – silver nanoparticles hybrid using Palash (*Butea monosperma*) flower extract and investigation of antibacterial activity. Polym Bull. 2018;75:1949–1955. https://doi.org/10.1007/s00289-017-2137-5
30. Taurozzi JS, Hackley VA, Wiesner MR. Ultrasonic dispersion of nanoparticles for environmental, health and safety assessment issues and recommendations. Nanotoxicology. 2011;5:711–729. https://doi.org/10.3109/17435390.2010.528846
31. Yadav MS, Singh N, Bobade SM. Zinc oxide nanoparticles and activated charcoal-based nanocomposite electrode for supercapacitor application. Ionics. 2018;24:3611–3630. https://doi.org/10.1007/s11581-018-2527-1
32. Malucelli LC, Massulo T, Magalhães WLE, Stofella NCF, Vasconcelos EC, Aurélio M, Filho SC, Murakami FS. Thermal and chemical characterization of Dicksonia sellowiana extract by means of thermal analysis. Rev bras farmacogn. 2018;28:626–630. https://doi.org/10.1016/j.bjp.2018.07.001
33. Mayedwa N, Khalil AT, Mongwaketsi N. The study of structural, physical and electrochemical activity of ZnO nanoparticles synthesized by green natural extracts of *Sageretia thea*. Nano Res Appl. 2017;3:1–9. https://doi.org/10.21767/2471-9838.100026
34. Pallela PNVK, Ruddaraju LK, Veerla SC, Matangi R, Kollu P, Ummey S, Pammi SVN. Synergetic antibacterial potential, dye degrading capability and biocompatibility of *Asperagus racemosus* root assisted ZnO nanoparticles. Mater Today Commun 25. 2020; 101574-1-101574-8. https://doi.org/10.1016/j.mtcomm.2020.101574
35. Skandalis N, Dimopoulou A, Georgopoulou A, Gallios N, Papadopoulos D, Tsipas D, Theologidis I, Michailidis N. The effect of silver nanoparticles size, produced using plant extract from *Arbutus unedo*, on their antibacterial efficacy. Nanomaterials. 2017;7:178–1-178 – 14. https://doi.org/10.3390/nano7070178
36. Kandjani AE, Tabriz MF, Pourabbas B. Sonochemical synthesis of ZnO nanoparticles: The effect of temperature and sonication power. Mater Res Bull. 2008;43:645–654. https://doi.org/10.1016/j.materresbull.2007.04.005
37. Tran QMT, Nguyen HAT, Doan V-D, Tran Q-T, Nguyen VC. Biosynthesis of zinc oxide nanoparticles using aqueous *Piper betle* leaf extract and its application in surgical sutures. J Nanomater. 2021; 8833864-1-8833864-15. https://doi.org/10.1155/2021/8833864

38. Wiśniewska M, Ostolska I, Szewczuk-Karpisz K, Chibowski S, Terpiłowski K, Gun'ko VM, Zarko VI. Investigation of the polyvinyl alcohol stabilization mechanism and adsorption properties on the surface of ternary mixed nanooxide AST 50 (Al_2O_3–SiO_2–TiO_2). J Nanopart Res. 2015;17:12-1-12–14. https://doi.org/10.1007/s11051-014-2831-2
39. Alias SS, Mohamad AA. ZnO nanocrystalline metal oxide semiconductor via sol gel method. In: Alias SS, Mohamad AA, editors. Synthesis of Zinc Oxide by Sol–Gel Method for Photoelectrochemical Cells. New York: Springer; 2014. pp. 1–8.
40. Wiśniewska M. Temperature effects on the adsorption of polyvinyl alcohol on silica. Cent Eur J Chem. 2012;10:1236–1244. https://doi.org/10.2478/s11532-012-0044-z
41. Eftekhari A, Ahmadian E, Panahi-Azar V, Hosseini H, Tabibiazar M, Dizaj SM. Hepatoprotective and free radical scavenging actions of quercetin nanoparticles on aflatoxin B1-induced liver damage: in vitro/in vivo studies. Artif Cell, Nanomed, Biotechnol. 2018;46:411–420. https://doi.org/10.1080/21691401.2017.1315427
42. Zheng J. Improving sample preparation methods to assess nanoparticle agglomeration using TEM. Microsc Microanal. 2014;20:1236–1237. https://doi.org/10.1017/S1431927614007910
43. Rakgotho T, Ndou N, Mulaudzi T, Iwuoha E, Mayedwa N, Ajayi RF. Green-synthesized zinc oxide nanoparticles mitigate salt stress in *Sorgum bicolor*. Agriculture. 2022;12:597–1-597 – 16. https://doi.org/10.3390/agriculture12050597
44. Kang MG, Khan F, Jo DM, Oh DK, Tabassum N, Kim YM. Antibiofilm and antivirulence activities of gold and zinc oxide nanoparticles synthesized from kimchi-isolated *Leuconostoc* sp. strain C2. Antibiotics. 2022;11:1524-1-1524-23. https://doi.org/10.3390/antibiotics11111524
45. Deshmukh AR, Gupta A, Kim BS. Ultrasound assisted green synthesis of silver and iron oxide nanoparticles using fenugreek seed extract and their enhanced antibacterial and antioxidant activities. Biomed Res Int 2019;1714358-1-1714358-14. https://doi.org/10.1155/2019/1714358
46. Baptista PV, McCusker MP, Carvalho A, Ferreira, DA, Mohan NM, Martins M, Fernandes AR. Nano-strategies to fight multidrug resistant bacteria-A Battle of the Titans. Front Microbiol. 2018;9:1–26. https://doi.org/10.3389/fmicb.2018.01441
47. Ikuma K, Decho AW, Lau BLT. When nanoparticles meet biofilms - Interactions guiding the environmental fate and accumulation of nanoparticles. Front Microbiol. 2015;6:1–6. https://doi.org/10.3389/fmicb.2015.00591
48. Shkodenko L, Kassirov I, Koshel E. Metal oxide nanoparticles against bacterial biofilms: Perspectives and limitations. Microorganisms. 2020;8:1–21. https://doi.org/10.3390/microorganisms8101545

Figures

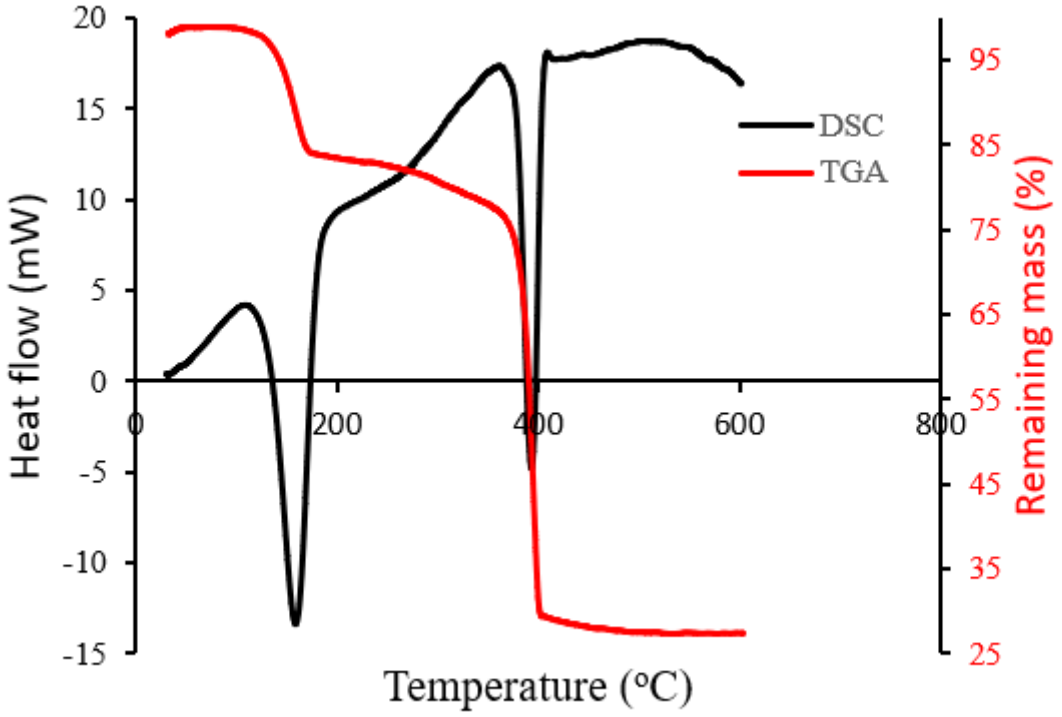

Figure 1

DSC/TGA thermograms of biosynthesized zinc nanoparticle specimen from preliminary experiment

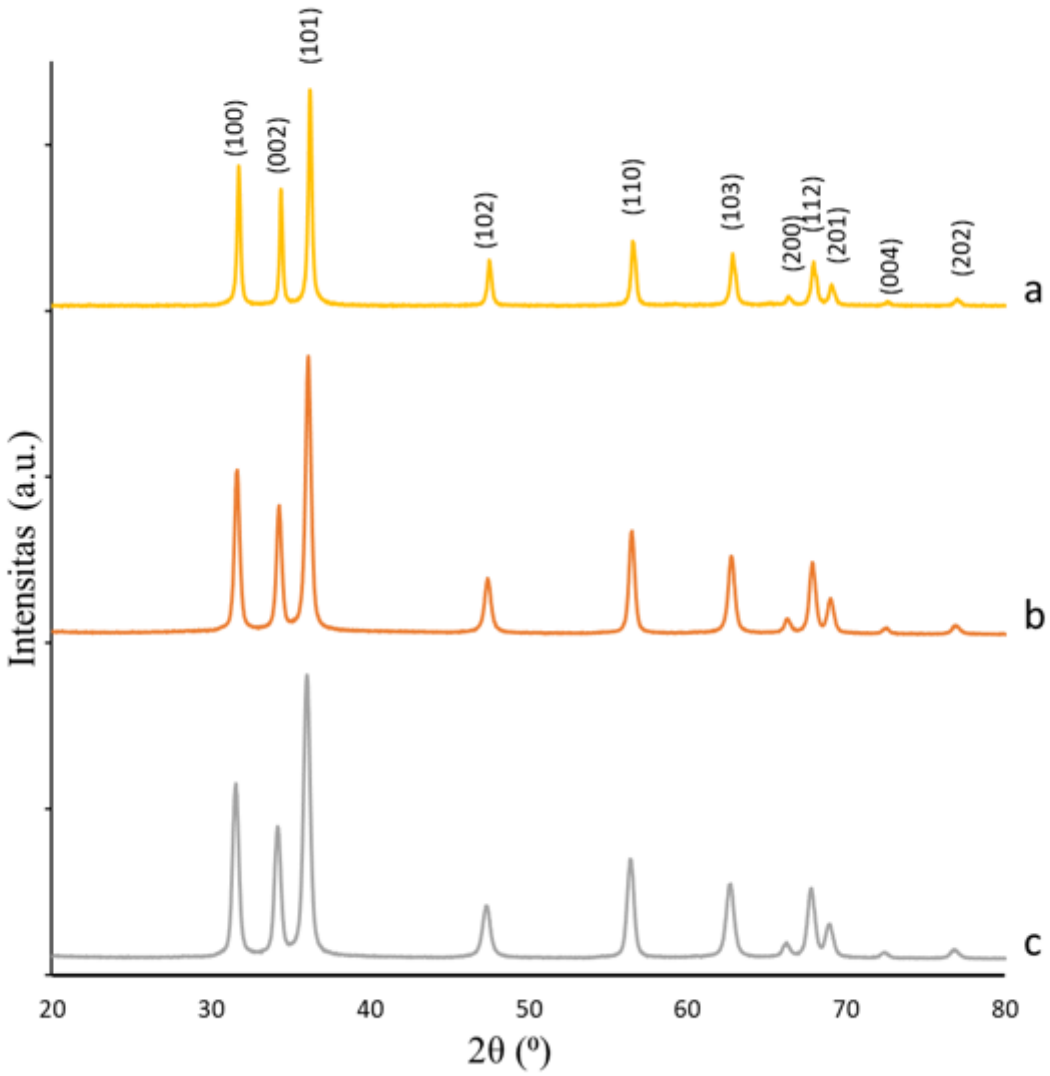

Figure 2

X-ray diffractograms of (**a**) commercial ZnO nanoparticle (Rahayu 2019) (**b**) biosynthesized ZnO nanoparticle with chemical deagglomeration (**c**) biosynthesized ZnO nanoparticle with physical deagglomeration. Biosynthesized specimens were calcined at 375 °C for 1 hour.

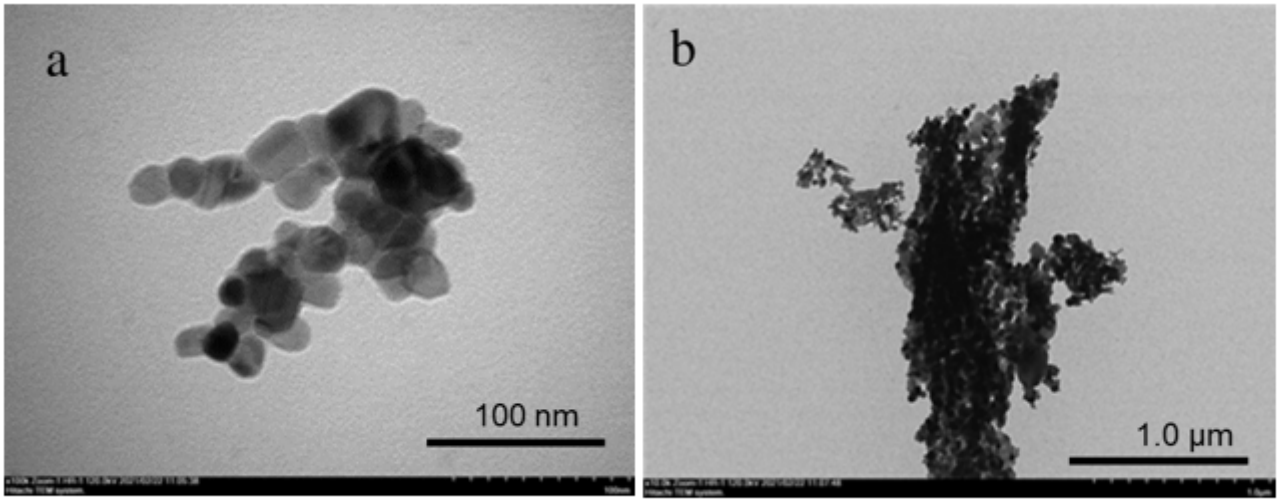

Figure 3

TEM image of ZnO nanoparticle specimen from Run no.2 (physical deagglomeration, 30 °C synthesis temperature, precursor / extract ratio = 0.5, magnification) (a) 100000×, and (b) 10000× magnification

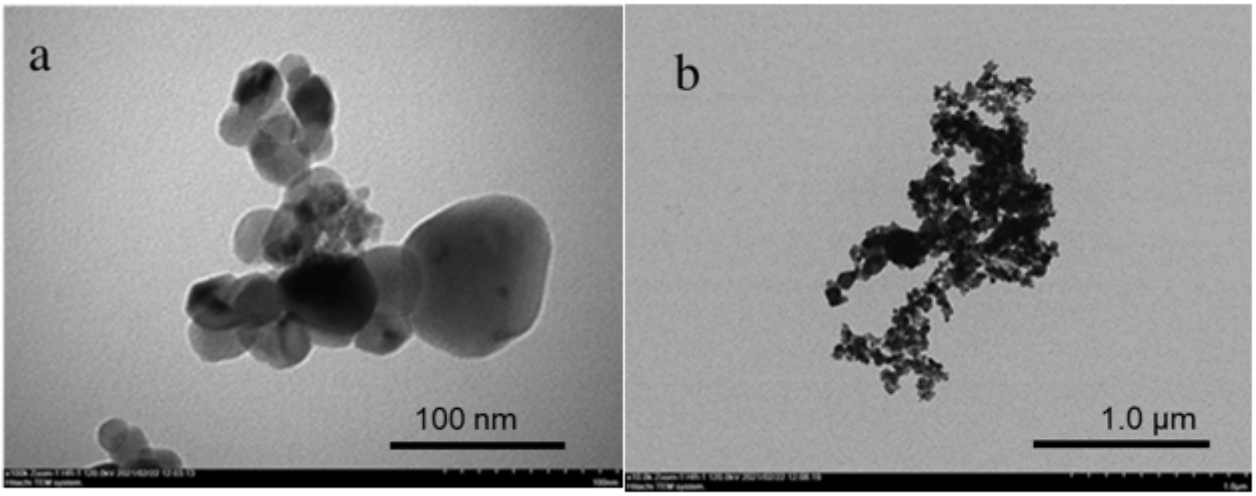

Figure 4

TEM image of ZnO nanoparticle specimen from Run no.3 (chemical deagglomeration, 60 °C synthesis temperature, precursor / extract ratio = 0.5) (a) 100000×, and (b) 10000× magnification

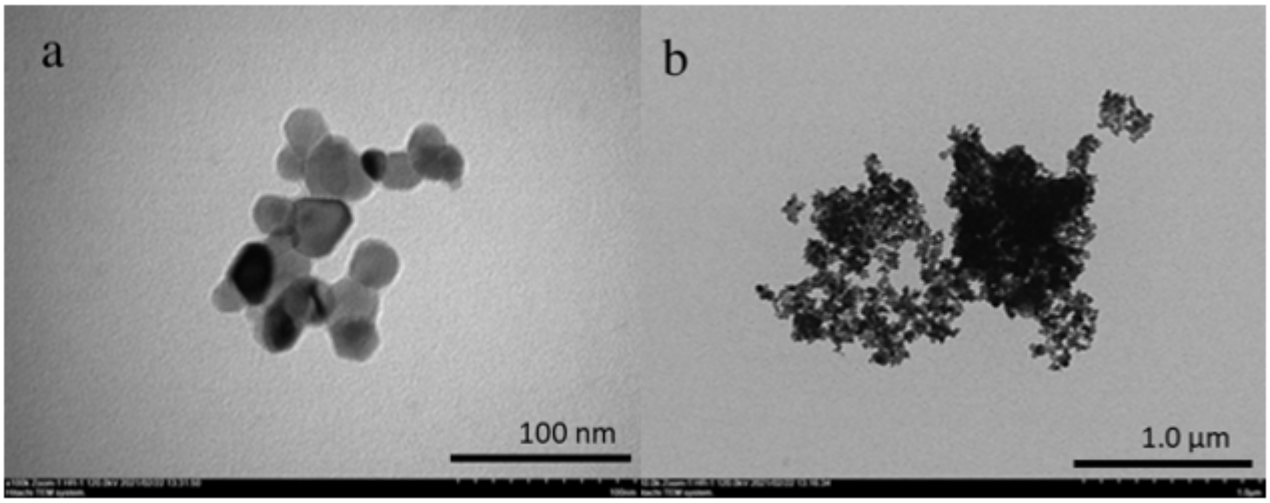

Figure 5

TEM image of ZnO nanoparticle specimen from Run no.5 (chemical deagglomeration, 30 °C synthesis temperature, precursor / extract ratio = 2.0) (a) 100000x, (b) 10000x magnification

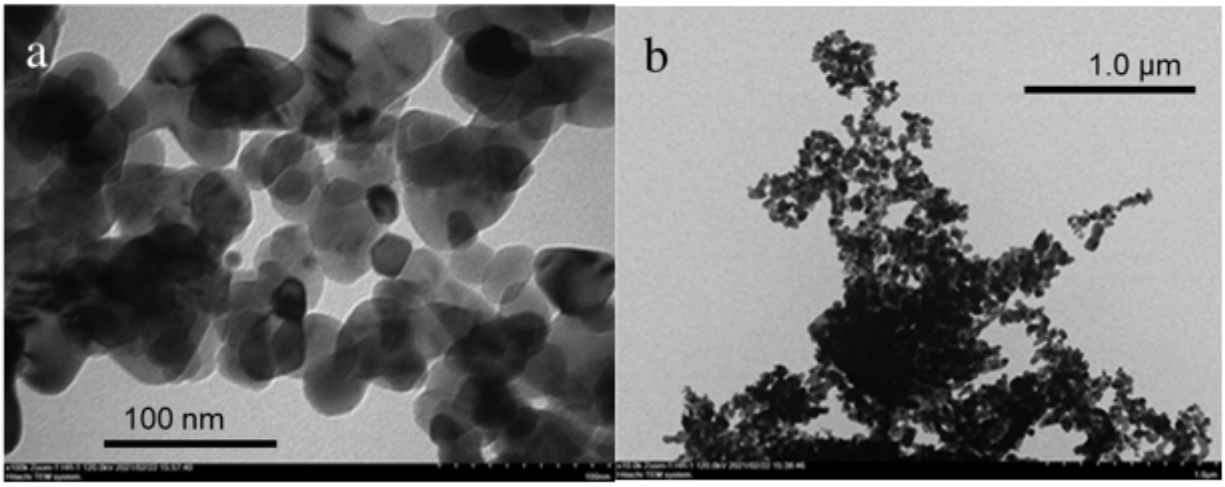

Figure 6

TEM image of ZnO nanoparticle specimen from Run no.8 (physical deagglomeration, 60 °C synthesis temperature, precursor / extract ratio = 2.0) (a) 100000x, (b) 10000x magnification

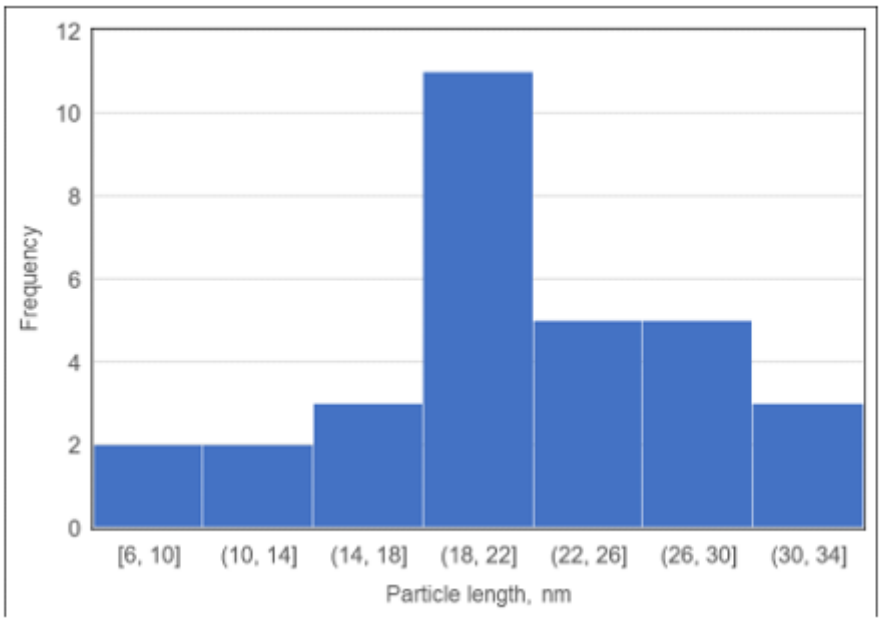

Figure 7

Particle size distribution obtained from image analysis of specimen from Run no. 5 using ImageJ freeware.

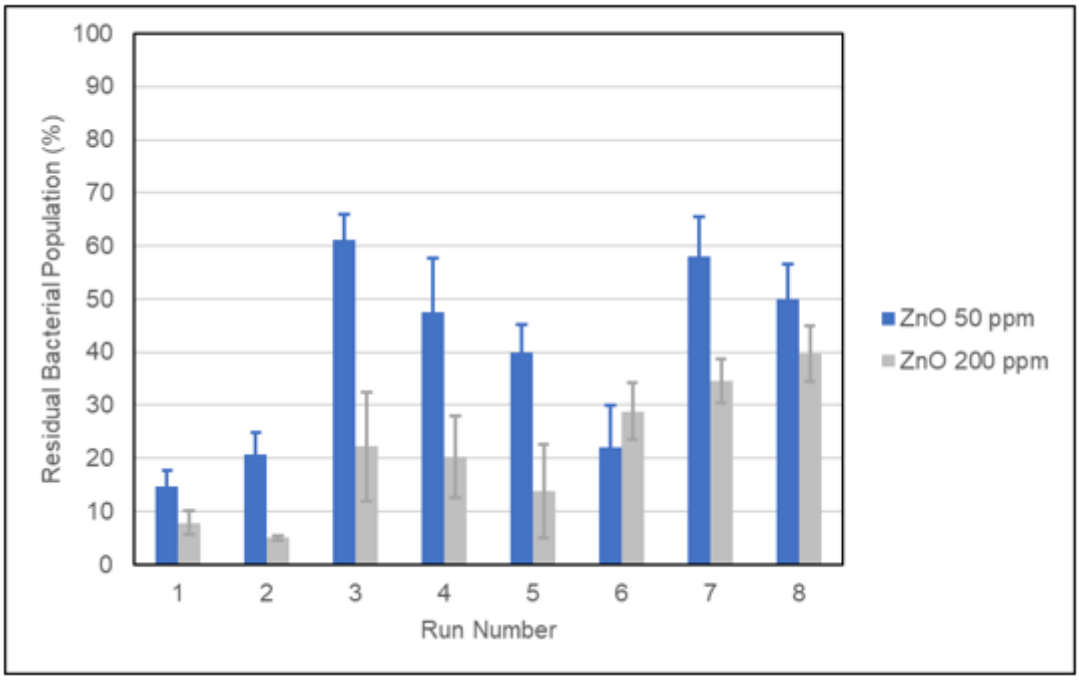

Figure 8

Residual *E.coli* biofilm population after 4.5 hrs of incubation in the presence of biosynthesized ZnO nanoparticles.

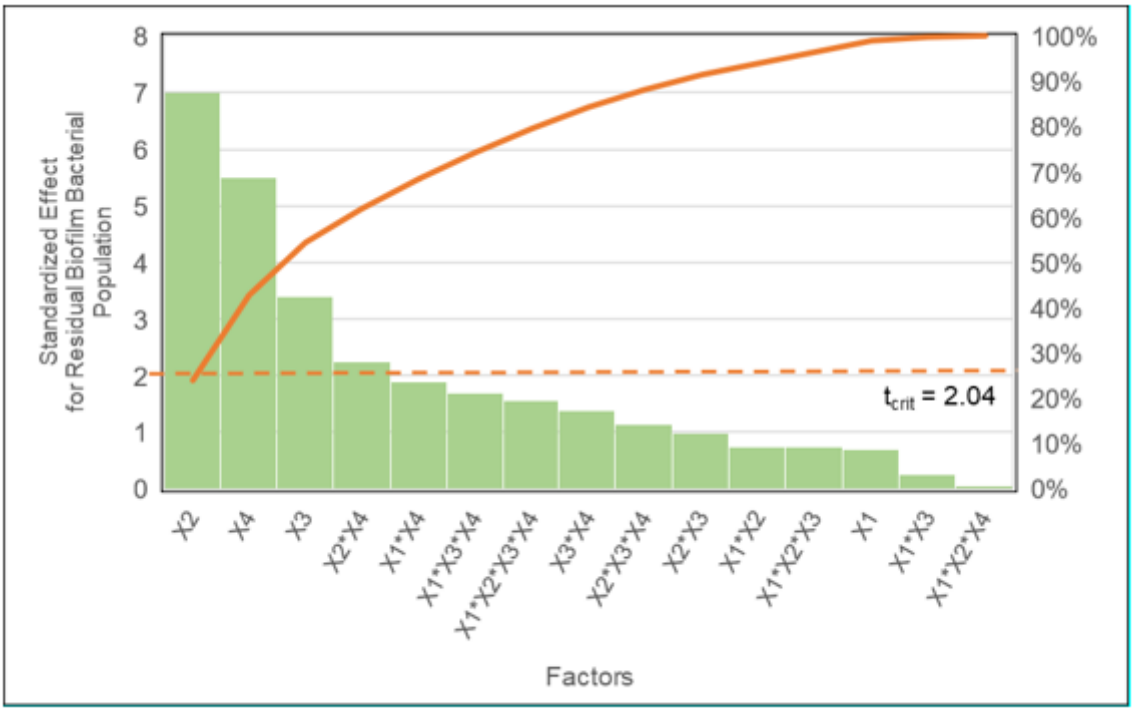

Figure 9

Pareto plot of effects in full model ANOVA treatment of antibacterial activity as measured by residual biofilm bacterial population at 95% confidence level (X_1 = deagglomeration method, X_2 = synthesis temperature, X_3 = precursor / extract volumetric ratio, X_4 = nanoparticle dose)